Electronic Supplementary Information for:

Heavy-Atom Effect on the Thermally Activated Delayed Fluorescence Property of Naphthalimide-Phenoselenazine Electron Donor-Acceptor Dyads: Electron Transfer and Intersystem Crossing

Peiwen Jiang,[a,b] Haotian Bai,[c] Yuying Pei,[a] Antonio Toffoletti,[d] Jianzhang Zhao,*[a] Yanqin Li,*[b] Yan Wan,*[c] and Antonio Barbon*[d]

[a] State Key Laboratory of Fine Chemicals, Frontier Science Center for Smart Materials, School of Chemical Engineering, Dalian University of Technology, Dalian 116024, P. R. China.
*Email: zhaojzh@dlut.edu.cn

[b] School of Chemistry, Dalian University of Technology, Dalian 116024, P. R. China.
*Email: liyanqin@dlut.edu.cn

[c] College of Chemistry, Beijing Normal University, Beijing 100875, P. R. China.
*Email: wanyan@bnu.edu.cn

[d] Dipartimento di Scienze Chimiche, Università degli Studi di Padova, Via Marzolo 1, 35131 Padova, Italy. *Email: antonio.barbon@unipd.it

Index

1. Experimental Section

1.1. General Methods. All of the chemicals used in the synthesis are analytically pure and were used as received. Solvents were dried and distilled prior to use. ^{1}H spectra were recorded on the Bruker Avance spectrometers at 400 MHz. The chemical shifts are reported in parts per million (ppm) relative to TMS, with the residual solvent peak used as a reference. The mass spectra were measured by MALDI-TOF MS spectrometer. UV–vis absorption spectra were measured on a UV–2550 spectrophotometer (Shimadzu Ltd., Japan). The fluorescence emission spectra were recorded with a FS5 spectrofluorometer (Edinburgh Instruments, U.K.). Luminescence lifetimes were measured on OB920 luminescence lifetime spectrometer (Edinburgh Instruments, U.K.). The fluorescence quantum yields (Φ_F) were measured with the C13534-11 Quantaurus-QY Plus UV-NIR absolute PL quantum yield spectrometer (Hamamatsu Ltd., Japan).

1.2. Single crystal X-ray diffraction. Single crystals of **NI-PXZ** and **NI-PSeZ** were obtained by slow evaporation of the *n*-hexane (HEX)/chloroform ($CHCl_3$) solution. The X-ray diffraction data of the single crystals were collected on a Bruker AXS SMART APEX II CCD diffractometer with graphite–monochromatized Mo Kα radiation (λ = 0.71073 Å) at 296K (**NI-PXZ** and **NI-PSeZ**), using the SMART and SAINT programs. The X-ray diffraction data were analyzed by the ShelXT structure solution program using Intrinsic Phasing and refined with the ShelXL refinement package using least squares minimization implemented in Olex2.[1] CCDC No. 2476452 (**NI-PXZ**) and 2476453 (**NI-PSeZ**) contain the supplementary crystallographic data for this paper and the data can be freely obtained from the Cambridge Crystallographic Data Centre.

1.3. Singlet Oxygen Quantum Yield. Singlet oxygen quantum yields (Φ_Δ) of compounds were measured with 1,3-Diphenylisobenzofuran (DPBF) as singlet oxygen scavenger. The $^1O_2$ production was monitored by following the absorbance of DPBF at 414 nm. For calculation of singlet oxygen quantum yield (Φ_Δ), the following equation S1 was used:

$$\Phi_{\mathrm{sam}} = \Phi_{\mathrm{std}} \left(\frac{1-10^{-A_{\mathrm{std}}}}{1-10^{-A_{\mathrm{sam}}}}\right)\left(\frac{m_{\mathrm{sam}}}{m_{\mathrm{std}}}\right)\left(\frac{\eta_{\mathrm{sam}}}{\eta_{\mathrm{std}}}\right)^2 \quad \text{(S1)}$$

In the above equation, "std" and "sam" stands for the standard and the sample. Φ, A, m and η represent the singlet oxygen quantum yield, the absorbance at excitation wavelength, the

slope of the absorbance of DPBF at 414 nm changing against irradiation time, and the refractive index of the solvent used for measurement, respectively.

1.4. Electrochemical studies. The cyclic voltammetry curves were recorded by a CHI610D electrochemical workstation (CHI instruments Inc., Shanghai, China). The counter electrode was a platinum electrode and the working electrode was a glassy carbon electrode. The ferrocenium/ferrocene (Fc^+/Fc) redox couple was used as the internal reference. Spectroelectrochemistry measurements were performed using a CHI610D electrochemical workstation (CHI instruments Inc., Shanghai, China) for potential control and an Agilent 8453 UV–vis spectrophotometer (Agilent Technologies Inc., USA) for spectra recording. The study was carried out using a quartz electrochemical cell with a path length of 0.1 cm. Gauze platinum was used as the working electrode and platinum wire as the counter electrode. In both cases, the reference electrode was the $Ag/AgNO_3$ (0.1 M in acetonitrile (ACN)) couple and the supporting electrolyte was the 0.10 M $Bu_4N[PF_6]$. Samples were deaerated with N_2 for about 15 min before measurement, and the N_2 atmosphere was maintained during the measurement.

1.5. Nanosecond transient absorption spectroscopy. The ns-TA spectra were measured with a LP980 laser flash photolysis spectrometer (Edinburgh Instruments, U.K.). All samples were purged with N_2 for 15 min, and excited with a nanosecond pulsed laser (Surelite Ⅰ−10, USA; the wavelength is tunable in the range of 210−2400 nm). The laser energy is about 10 mJ per pulse and the signal was digitized using a Tektronix TDS 3012B oscilloscope and the data were analyzed by L900 software.

1.6. Femtosecond transient absorption spectroscopy. Femtosecond Transient Absorption (fs-TA) measurements were performed with a Harpia-TA (Light Conversion) ultra-fast transient absorption (TA) spectrometer. The femtosecond experiments were conducted by employing a Ti/sapphire laser system with a pulse duration of approximately 40 fs and a repetition rate of 1 kHz (800 nm, Coherent Astrella). The excitation wavelength was determined based on the steady-state UV–vis absorption spectra and generated using an optical parametric amplifier (TOPAS-C, Coherent). The magic angle between the probe and the direction of polarization of the pump beam is used. The data were analyzed by singular value decomposition and global analysis by employing the software Glotaran.[2]

1.7. Time-resolved electron paramagnetic resonance spectra. Samples at a concentration of 1.0×10^{-4} M were dissolved in TOL/(2-methyltetrahydrofuran, 2-MeTHF) = 3/1 (v/v). Time-resolved continuous-wave (CW) EPR spectra were recorded on an X-band EPR Elexsys E-580 spectrometer (Bruker) equipped with the dielectric ring X-Band ER 4118X-MD5-W1 resonator at 80 K. The samples were excited at a wavelength of 355 nm, a pulse energy of 2 mJ and frequency of 100 Hz. The spectra were simulated using the EasySpin package based on Matlab.[3]

1.8. DFT calculations. DFT calculations were performed by using the Gaussian 16 package.[4] The ground state geometries and orbital energies were optimized using DFT with the CAM-B3LYP/6-31G(d) and CAM-B3LYP/GENCP level. The triplet excited state energies of the compounds were calculated by time-dependent DFT (TD-DFT) with CAM-B3LYP functional and 6-31G(d) basis set based on the optimized ground state geometry. The calculation of the spin orbital coupling matrix elements (SOCMEs) of the compounds were performed at B3LYP/def2-TZVP level using the ORCA 6.0 programs. And the zero field splitting parameters (D and E), spin−spin and spin−orbit of the compounds were calculated at B3LYP/EPR-II level using the ORCA 6.0 programs.[9]

2. Synthesis of the Compounds

Scheme S1. Synthesis of the Compounds [a]

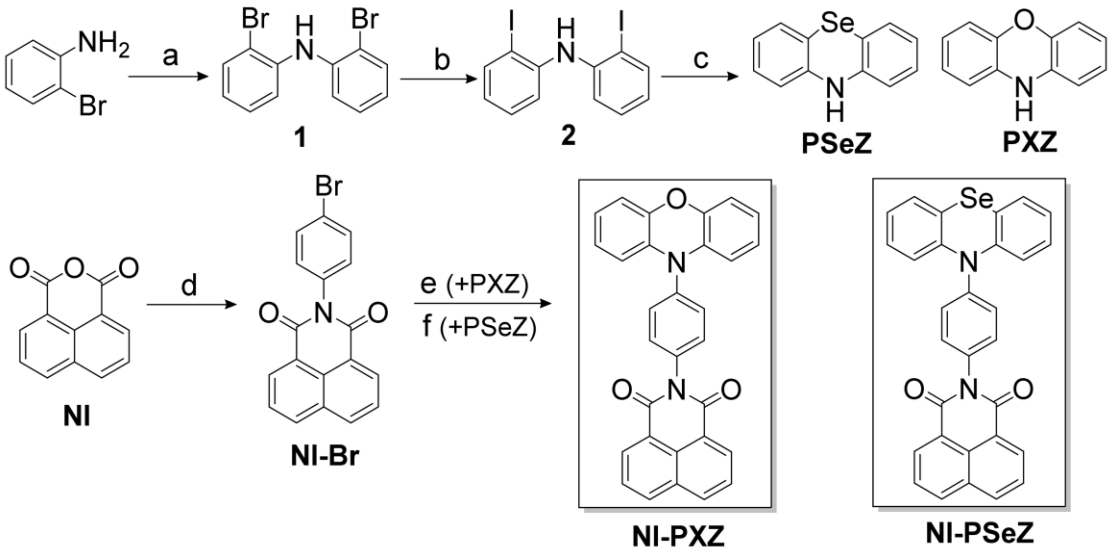

[a]Key: (a) 1,2-bromoiodobenzene, *t*-BuONa, $Pd_2(dba)_3$, 1,1-bis(diphenyphosphino)ferrocene (DPPF), toluene, 120 °C, 12 h, under N_2, yield: 81%; (b) CuI, NaI, *N,N′* -Dimethylethylendiamine, dioxane, 110 °C, 10 h, under N_2, yield: 79%; (c) Se, KOH, DMSO, 120 °C, 12 h, under N_2, yield: 70%; (d) 4-Bromoaniline, acetic acid, 120 °C, 9 h, under N_2, yield: 46%; (e) phenoxazine, $Pd(OAc)_2$, tri-*tert*-butylphosphine tetrafluoroborate, K_2CO_3, toluene, 120 °C, 5 h, under N_2, yield: 15%; (f) phenoselenazine, similar to step (e), yield: 18%.

2.1 Synthesis of 1.[5] The synthesis of compound **1** was referred to the literature. In a 100 mL two-neck bottle, 2-bromoaniline (1.7 g, 10.0 mmol), 2-bromoiodobenzene (1.5 mL, 12.0 mmol) and t-BuONa (1.4 g, 14.0 mmol) were dissolved in dry toluene (25 mL). Then, $Pd_2(dba)_3$ (458.0 mg, 0.5 mmol) and DPPF (554.0 mg, 1.0 mmol) were added under N_2 atmosphere and purged with N_2 for 20 minutes. The mixture was stirred at 120 °C for 12 h. After cooling, the organic layer was extracted with ethyl acetate (3 × 40 mL) by washing with brine, then dried over anhydrous Na_2SO_4 and the solvent was evaporated under reduced pressure. The crude product was purified by column chromatography pure petroleum ether (PE) yielding the compound. Compound **1** was obtained as colorless oil. Yield: 2.5 g (81%). ^{1}H NMR (DMSO-d_6, 400 MHz): δ = 7.64 (d, 2H, J = 8.0 Hz), 7.29 (t, 2H, J = 8.0 Hz), 7.06 (d, 2H, J = 8.0 Hz), 7.01 (s, 1H), 6.93 (t, 2H, J = 8.0 Hz).

2.2 Synthesis of 2.[5] The synthesis of compound **2** was referred to the literature. In a 100 mL two-neck bottle, compound **1** (1.6 g, 5.0 mmol), CuI (95.0 mg, 0.5 mmol), NaI (3.0 g, 20.0 mmol) and *N, N′* -Dimethylethylendiamine (0.1 mL, 2.0 mmol) were mixed in dry dioxane (20 mL). The mixture was refluxed under N_2 atmosphere and stirred for 10 h. After cooling to room temperature, water was added to the mixture. The mixture was extracted with dichloromethane (DCM, 3 × 30 mL). The organic layer was dried over anhydrous Na_2SO_4 and the solvent was evaporated under reduced pressure. The crude product was purified by column chromatography pure PE yielding the compound. Compound **2** was obtained as colorless oil. Yield: 1.6 g (79%). ^{1}H NMR (DMSO-d_6, 400 MHz): δ = 7.64 (d, 2H, J = 7.9 Hz), 7.29 (t, 2H, J = 7.9 Hz), 7.06 (m, 3H), 6.95 (t, 2H, J = 8.0 Hz).

2.3 Synthesis of PSeZ.[6] The synthesis of compound **PSeZ** was referred to the literature. In a 100 mL two-neck bottle, compound **2** (3.4 g, 8.0 mmol), Se (1.2 g, 16.0 mmol) and KOH (1.8 g, 32.0 mmol) were mixed in dry DMSO (30 mL). The mixture was heated to 120 °C under N_2 atmosphere and stirred for 12 h. After cooling, sat. NH_4Cl solution was added, and the mixture was extracted with DCM (3 × 30 mL). The organic layer was dried over anhydrous Na_2SO_4 and the solvent was evaporated under reduced pressure. The crude product was purified by column chromatography (silica gel, PE: DCM = 2: 1, v: v). Compound **PSeZ** was obtained as yellow solid. Yield: 1.4 g (70%). ^{1}H NMR (DMSO-d_6, 400 MHz): δ = 8.58 (s, 1H), 7.10 (d, 2H, J = 7.9 Hz), 7.04 (t, 2H, J = 8.0 Hz), 6.78−6.75 (m, 4H).

2.4 Synthesis of NI-Br.[7] The synthesis of compound **NI-Br** was referred to the literature. In a 100 mL two-neck bottle, 1,8-naphthalic anhydride (2.0 g, 10.0 mmol) and 4-bromoaniline (2.0 g, 12.0

mmol) were mixed in acetic acid (20 mL). The mixture was heated to 120 °C under N_2 atmosphere and stirred for 9 h. After cooling to room temperature, the reaction mixture was poured into water (30 mL) and extracted with DCM (3 × 30 mL). Then, the organic layer was washed with saturated salt solution and dried over anhydrous Na_2SO_4. Solvent was removed under reduced pressure and crude product was purified by column chromatography (silica gel, PE: DCM = 1: 1, v: v). Compound **NI-Br** was obtained as white solid. Yield: 1.6 g (46%). ^{1}H NMR ($CDCl_3$, 400 MHz): δ = 8.65 (d, 2H, J = 8.0 Hz), 8.29 (d, 2H, J = 7.9 Hz), 7.82 (t, 2H, J = 7.9 Hz), 7.68 (d, 2H, J = 8.0 Hz), 7.22−7.19 (m, 2H).

2.5 Synthesis of NI-PXZ.[8] In a 50 mL two-neck bottle, **NI-Br** (175.5 mg, 0.50 mmol) and PXZ (136.5 mg, 0.75 mmol) were mixed in dry toluene (TOL, 10 mL). Then, $Pd(OAc)_2$ (22.4 mg, 0.10 mmol), K_2CO_3 (276.0 mg, 2.0 mmol) and tri-*tert*-butylphosphine tetrafluoroborate (14.5 mg, 0.05 mmol) were added under N_2 atmosphere and the mixture was purging with N_2 for 20 min. The mixture was refluxed and stirred for 5 h. After cooling to room temperature, DCM (10 mL) was added to the reaction mixture and then the mixture was poured into water. The mixture was extracted with DCM (3 × 10 mL). The organic layer was dried over anhydrous Na_2SO_4 and the solvent was removed under reduced pressure. The crude product was purified by column chromatography (silica gel, DCM: PE = 1.5: 1, v: v). Compound **NI-PXZ** was obtained as orange red solid (70 mg, yield: 15%). m.p.: >250 °C. ^{1}H NMR ($CDCl_3$, 400 MHz) δ 8.69 (d, 2H, J = 7.8 Hz), 8.32 (d, 2H, J = 8.2 Hz), 7.84 (t, 2H, J = 7.7 Hz), 7.56 – 7.53 (m, 4H), 6.71 – 6.63 (m, 6H), 6.08 (s, 2H). ^{13}C NMR ($CDCl_3$, 125 MHz): δ = 159.57, 139.22, 134.32, 130.65, 129.83, 129.36, 127.09, 127.03, 126.91, 123.85, 122.45, 118.65, 117.95, 116.80, 110.67, 108.86, 72.51, 72.30, 72.09. HRMS (MALDI–TOF): calcd for $C_{30}H_{17}N_2O_3^+$, m/z 454.1311; found m/z 454.1297.

2.6 Synthesis of NI-PSeZ.[8] The synthesis procedure is similar to that of **NI-PXZ**. Compound **NI-PSeZ** was obtained as yellow solid (93 mg, yield: 18%). m.p.: >250 °C. ^{1}H NMR (DMSO-d_6, 400 MHz) δ 8.52 (d, 4H, J = 7.8 Hz), 7.91 (t, 2H, J = 7.9 Hz), 7.56 (d, 2H, J = 7.7 Hz), 7.41 (d, 2H, J = 8.2 Hz), 7.31 – 7.23 (m, 4H), 7.15 – 7.08 (m, 4H). ^{13}C NMR ($CDCl_3$, 125 MHz): δ = 159.72, 139.45, 138.26, 129.77, 129.58, 127.89, 127.03, 126.93, 125.82, 125.76, 125.17, 123.81, 122.80, 122.36, 122.34, 120.08, 119.92, 118.80, 118.11, 118.09, 72.51, 72.30, 72.09. HRMS (MALDI–TOF): calcd for $C_{30}H_{17}N_2O_2Se^+$, m/z 518.0527; found m/z 518.0513.

3. Molecular Structure Characterization Data

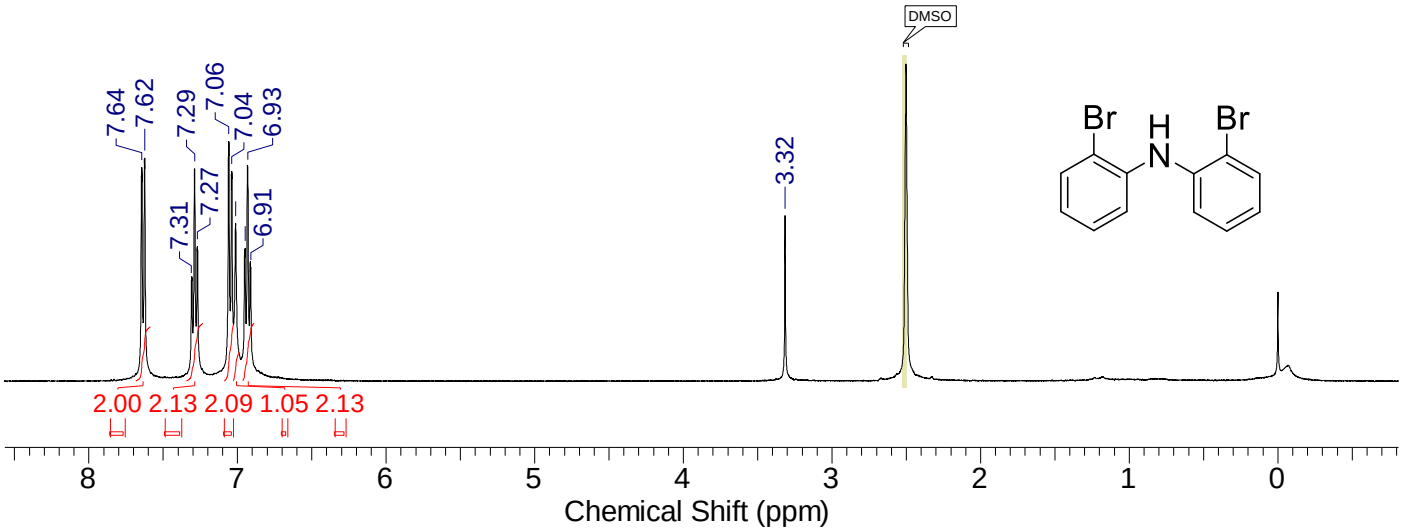

Figure S1. ^{1}H NMR spectrum of **1** (400 MHz, DMSO-d_6), 20 °C.

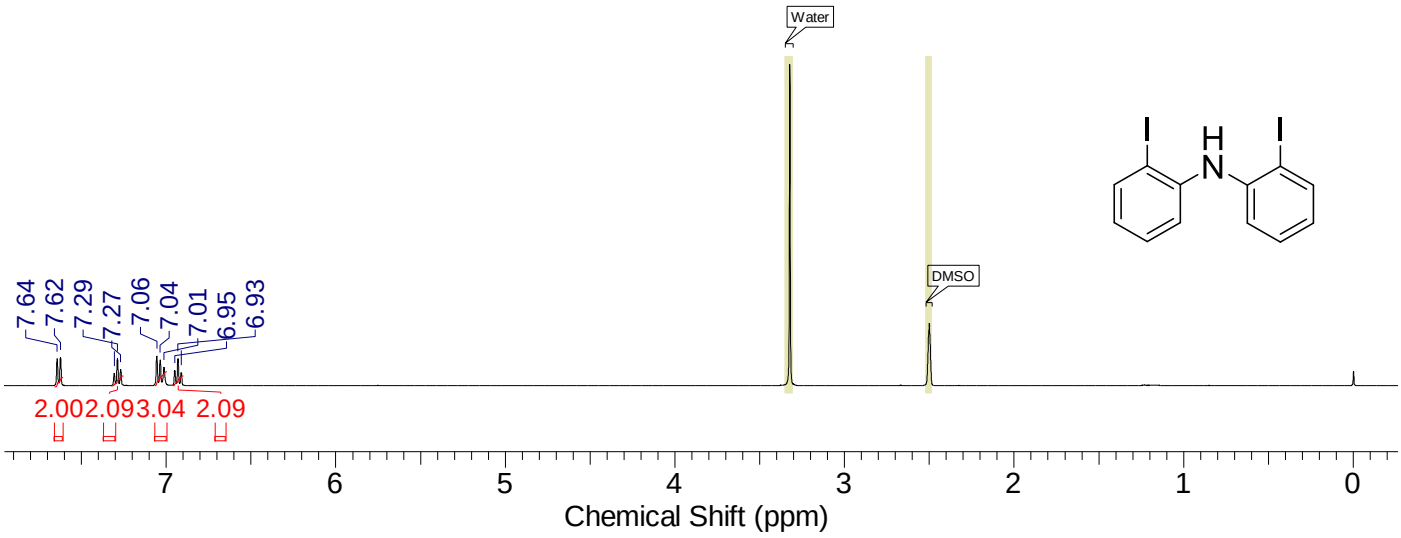

Figure S2. ^{1}H NMR spectrum of **2** (400 MHz, DMSO-d_6), 20 °C.

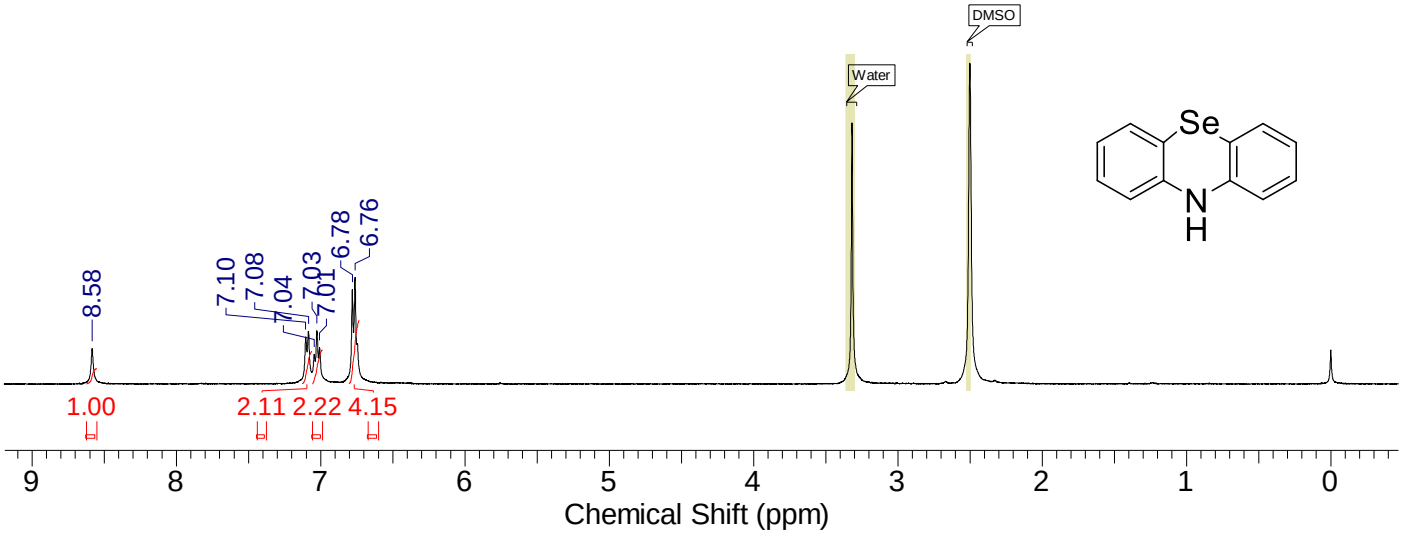

Figure S3. ^{1}H NMR spectrum of **PSeZ**(400 MHz, DMSO-d_6), 20 °C.

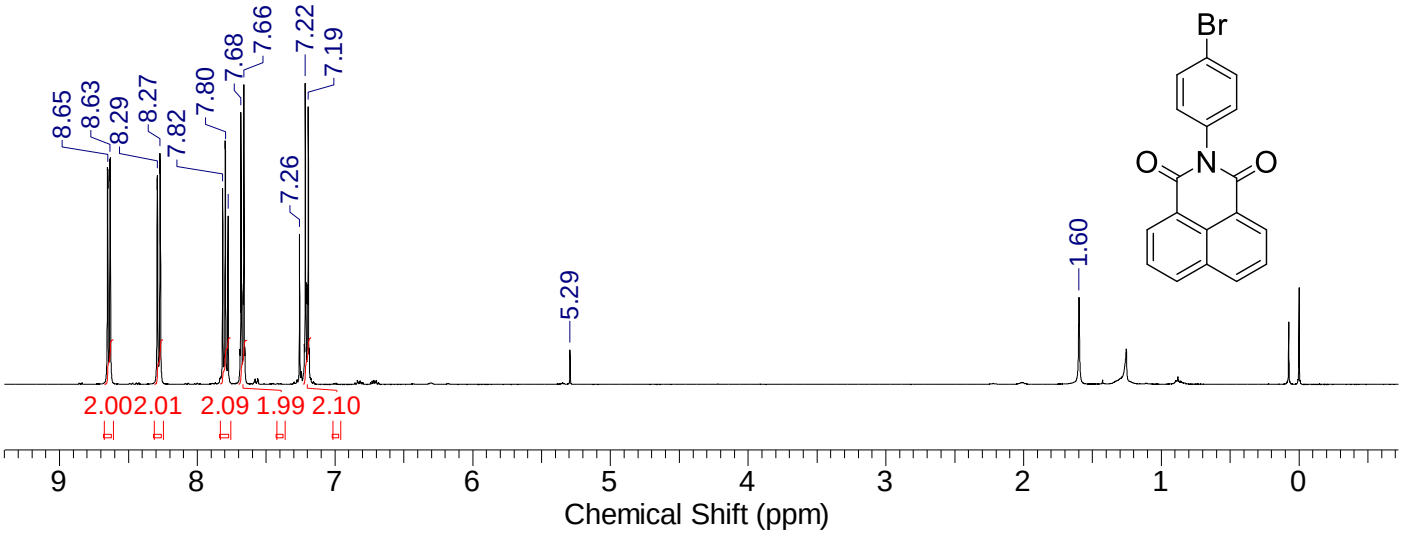

Figure S4. ^{1}H NMR spectrum of **NI-Br** (400 MHz, $CDCl_3$), 20 °C.

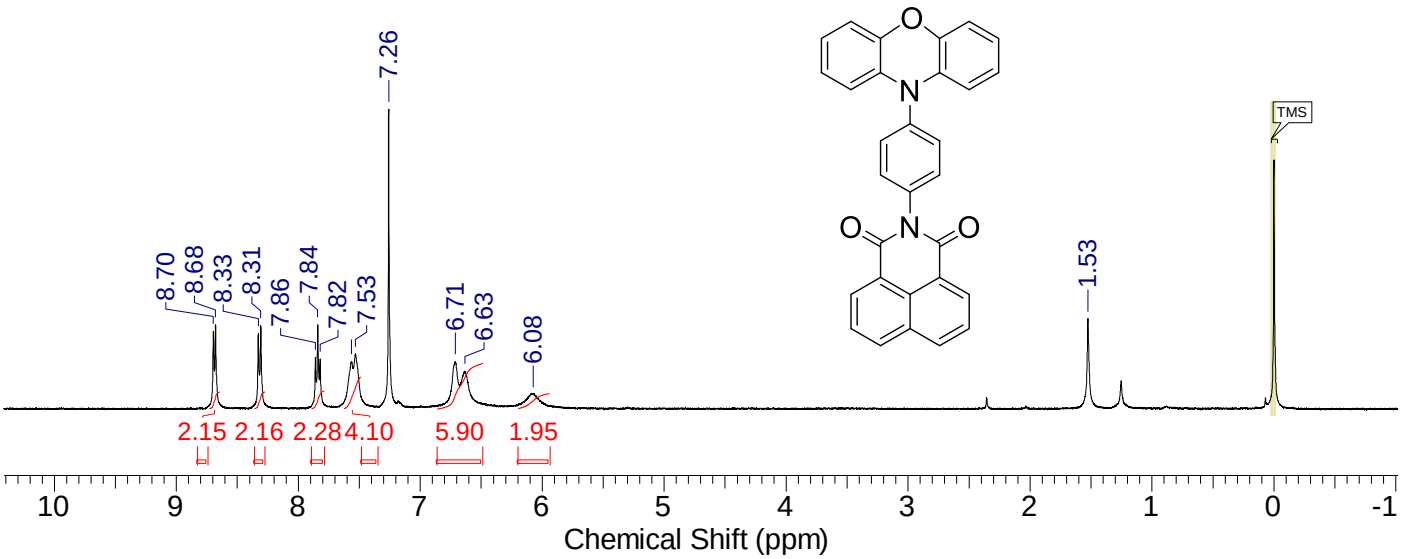

Figure S5. ^{1}H NMR spectrum of **NI-PXZ**(400 MHz, $CDCl_3$), 20 °C.

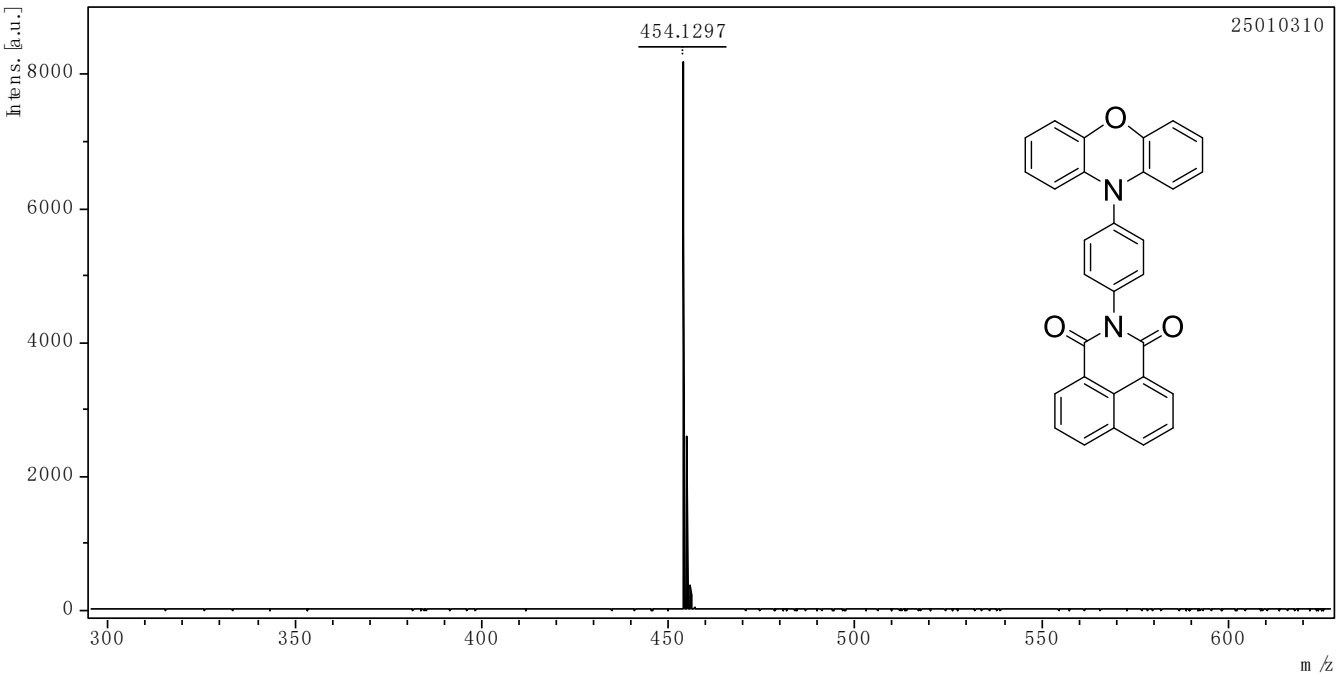

Figure S6. MALDI-TOF high resolution mass spectrum of **NI-PXZ**, 20 °C.

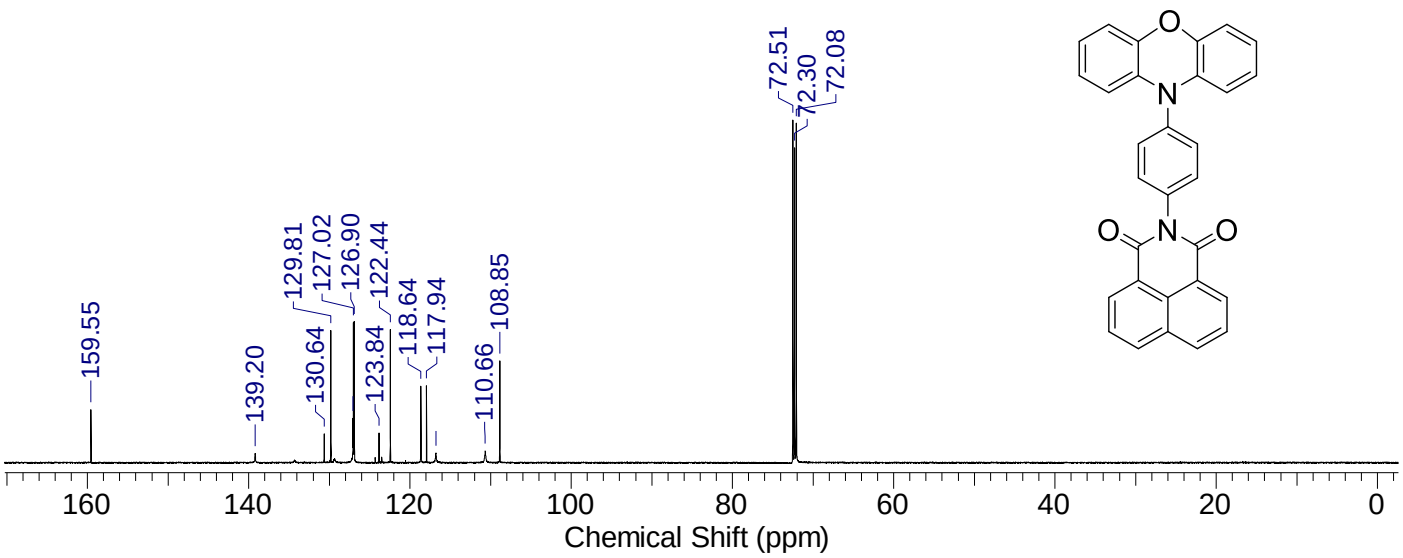

Figure S7. ^{13}C NMR spectrum of **NI-PXZ**(400 MHz, $CDCl_3$), 20 °C.

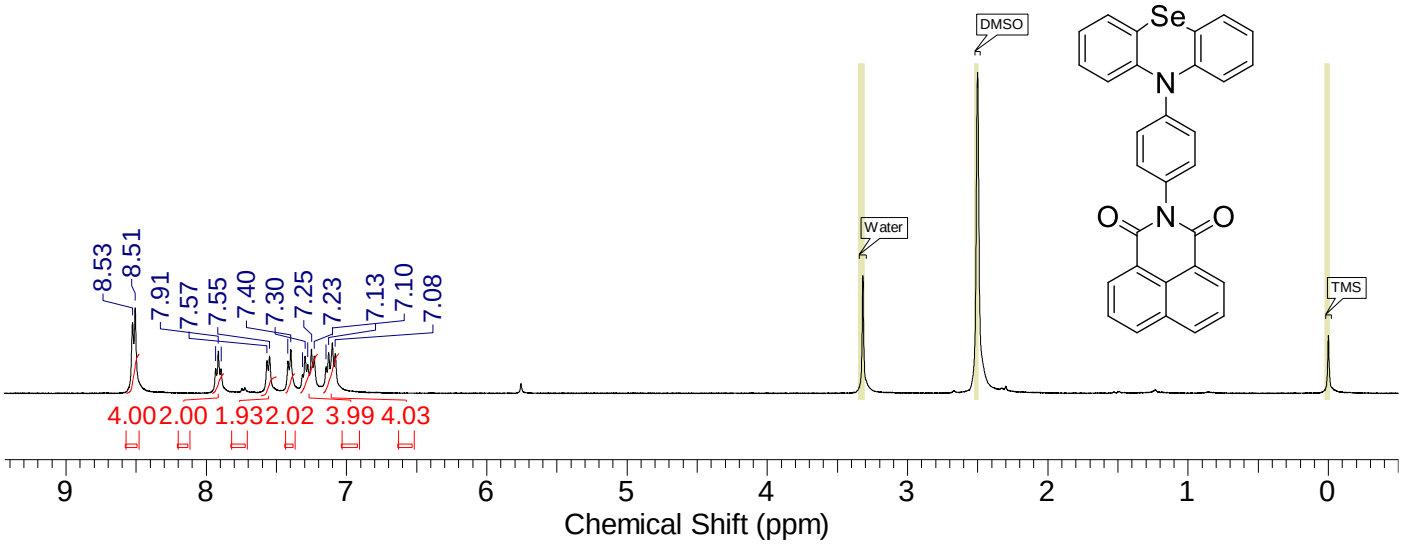

Figure S8. ^{1}H NMR spectrum of **NI-PSeZ**(400 MHz, DMSO-d_6), 20 °C.

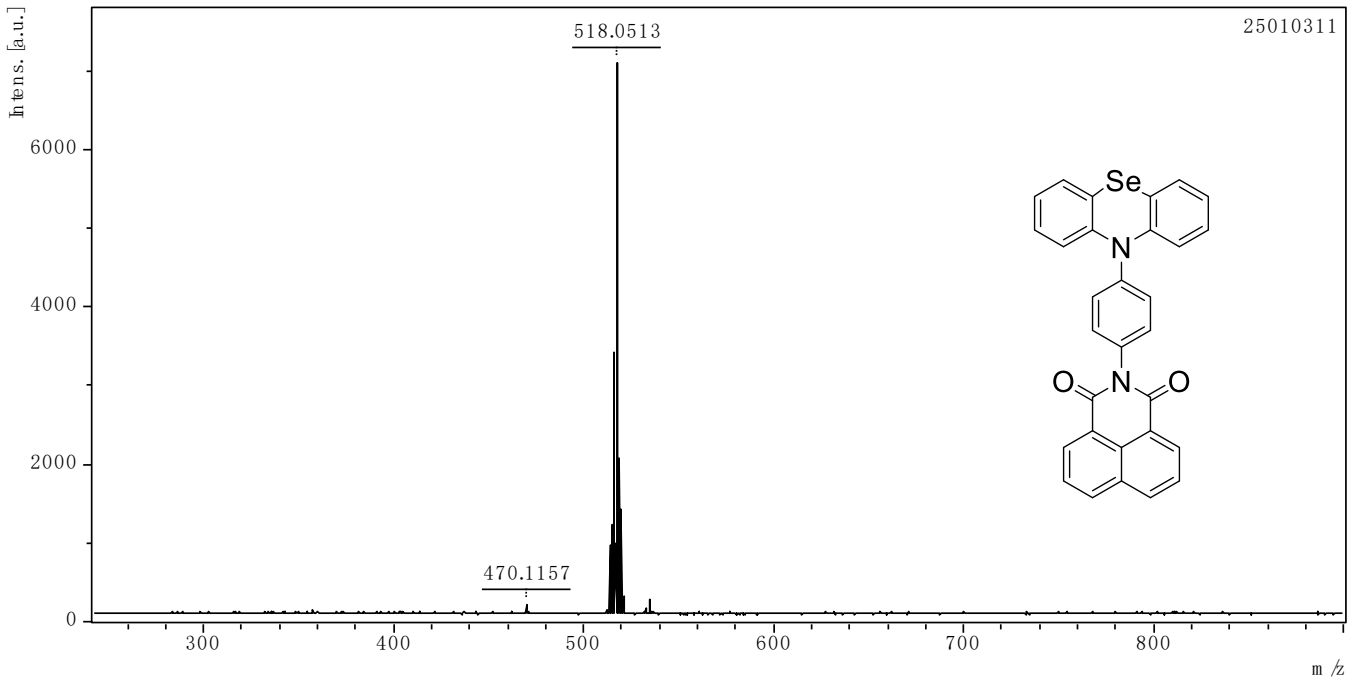

Figure S9. MALDI-TOF high resolution mass spectrum of **NI-PSeZ**, 20 °C.

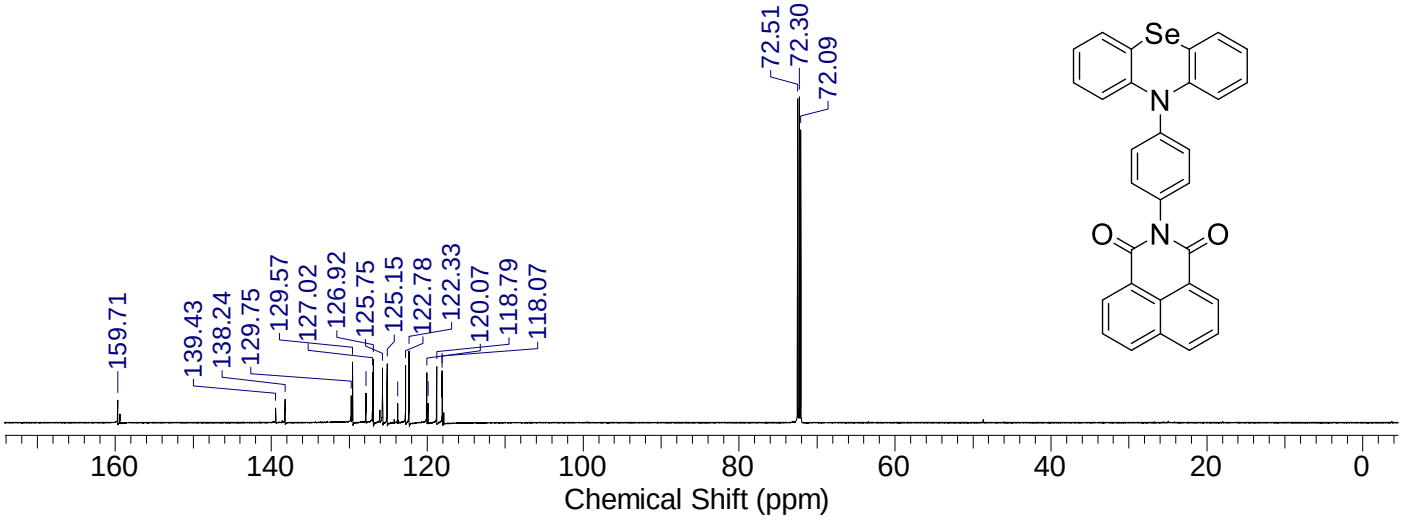

Figure S10. ^{13}C NMR spectrum of **NI-PSeZ**(400 MHz, $CDCl_3$), 20 °C.

4. Crystal Data of NI-PXZ and NI-PSeZ

Table S1. Crystallographic data for NI-PXZ (CCDC: 2476453) and NI-PSeZ (CCDC: 2476452)[a]

Complexes	**NI-PXZ**	**NI-PSeZ**
Sum formula	$C_{30}H_{18}N_2O_3$	$C_{30}H_{18}N_2O_2Se$
M (g mol^{-1})	454.43	517.42
Temperature / K	120	173
Crystal system	monoclinic	triclinic
Space group	P 21/n	P −1
a (Å)	13.0676(7)	11.4181(6)
b (Å)	13.2824(7)	13.0528(7)
c (Å)	14.8165(8)	16.1372(8)
α (deg)	90	70.758(2)
β (deg)	90.926(2)	89.034(2)
γ (deg)	90	78.292(2)
Volume / Å^3	2571.4(2)	2220.2(2)
Z	4	4
D_{calc} / g · cm^{-3}	1.482	1.548
Crystal size (mm)	0.1 × 0.08 × 0.06	0.5 × 0.5 × 0.5
F (000)	1176	1048
μ (Mo − Kα) / mm^{-1}	0.395	2.552
θ (deg)	27.495 / 2.059	68.596 – 2.905
Reflections collected	5833	8083
Independent reflections	4984	7589
Parameters	352	631
Largest diff. peak and hole (e Å^{-3})	0.716 / –0.589	1.337 / –0.802
Goodness of fit	1.052	1.016
R^a	0.0445	0.0448
$\omega R_2{}^a$	0.1198	0.1255

[a] $R = \sum \| F_o | - | F_c \| / \sum | F_o |$, $wR_2 = \left[\sum \left(w \left(F_o^2 - F_c^2 \right)^2 \right) / \sum \left(w \left(F_o^2 \right)^2 \right) \right]^{1/2}$ $\left[F_o > 4\sigma \left(F_o \right) \right]$. After repeated refinement, the wR_2 value is slightly larger, which is caused by poor crystal quality or weak diffraction points.

5. UV-vis Absorption and Fluorescence Emission Spectra

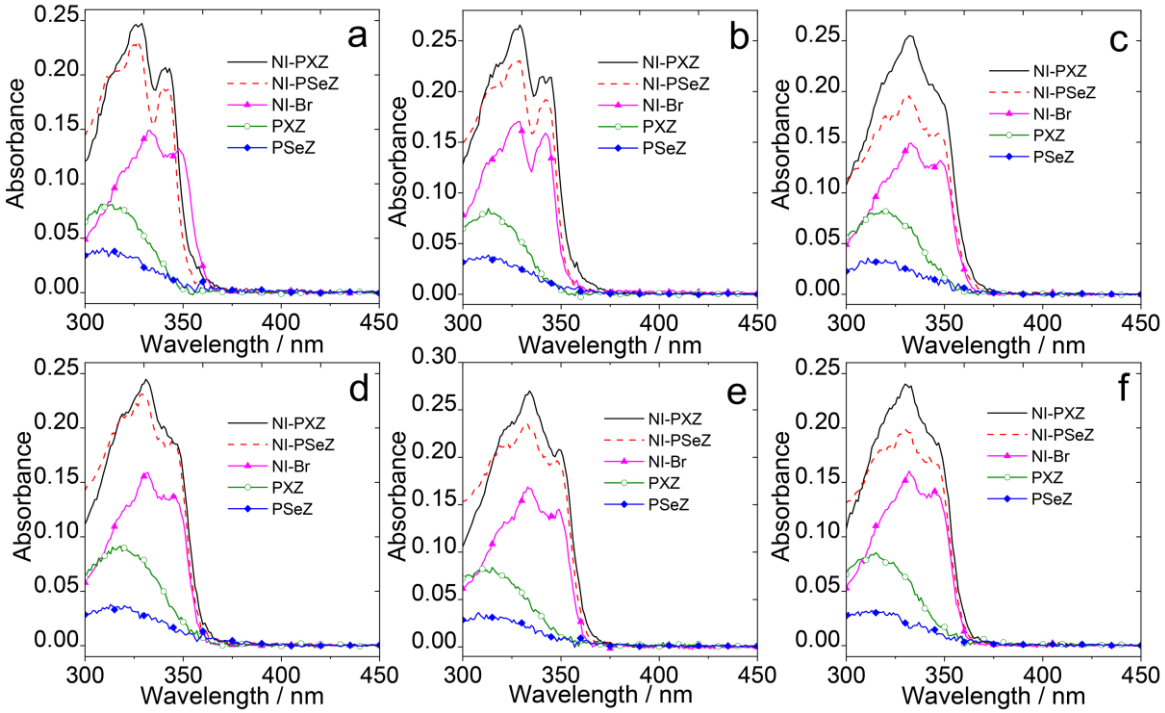

Figure S11. UV−vis absorption spectra of the compounds in (a) **CHX**, (b) **HEX**, (c) **TOL**, (d) **THF**, (e) **DCM** and (f) **ACN**. c = 1.0 × 10^{-5} M. 20 °C.

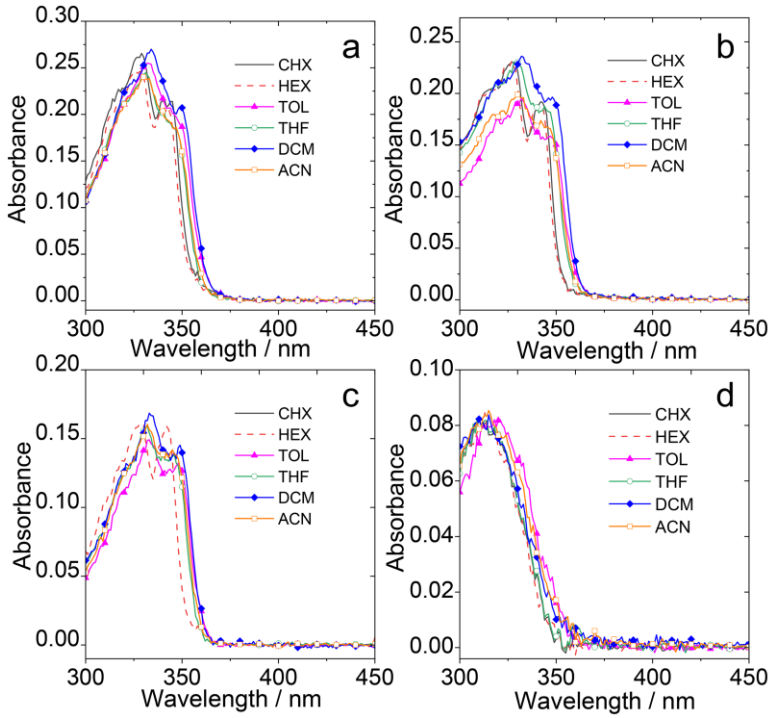

Figure S12. UV−vis absorption spectra of the compounds (a) **NI-PXZ**, (b) **NI-PSeZ**, (c) **NI-Br** and (d) **PXZ**. c = 1.0 × 10^{-5} M. 20 °C.

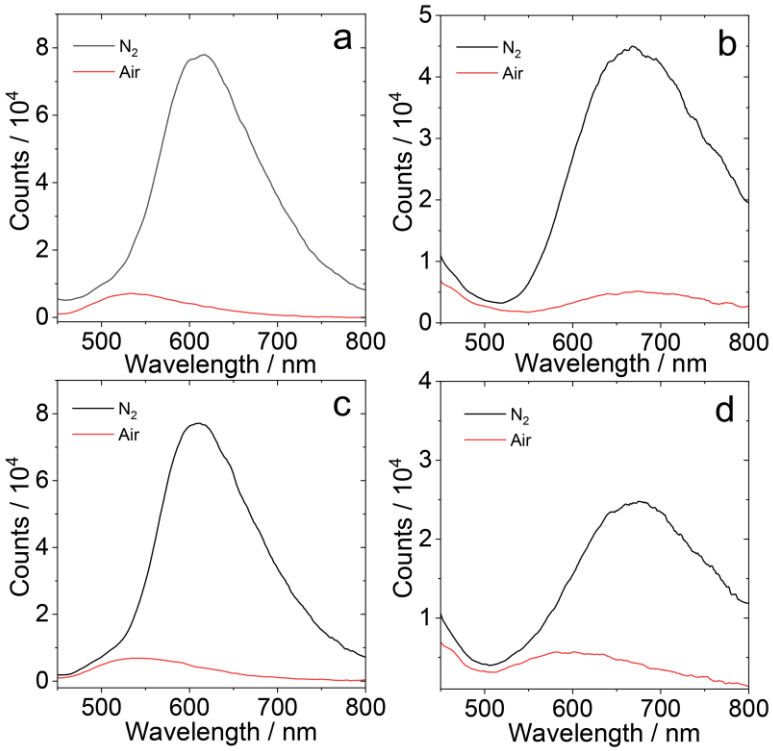

Figure S13. Fluorescence spectra of the **NI-PXZ** in (a) HEX, (b) TOL, **NI-PSeZ** in (c) HEX, (d) TOL. λ_{ex} = 340 nm. A = 0.10, 20 °C.

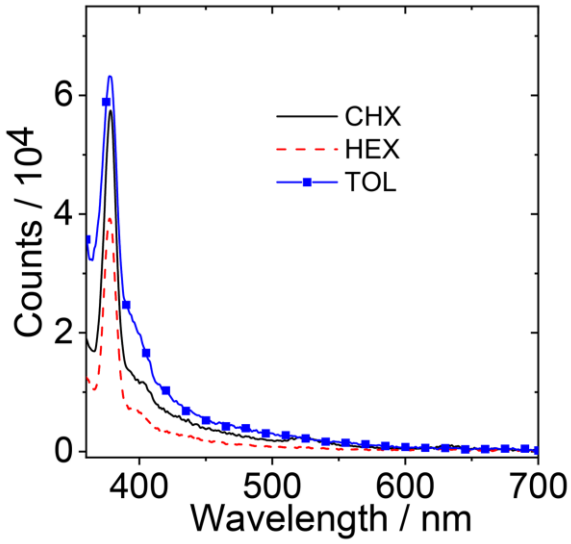

Figure S14. Fluorescence spectra of the **NI-Br** in different solvents under air atmosphere. λ_{ex} = 340 nm. A = 0.10, 20 °C.

6. Fluorescence Lifetime Spectra

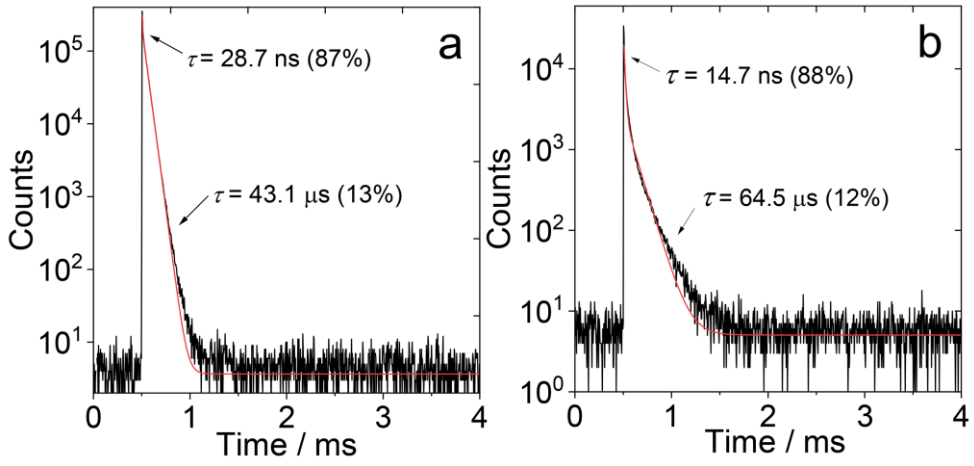

Figure S15. Fluorescence decay traces at 600 nm of (a) **NI-PXZ** and (b) **NI-PSeZ**, the short-life time was measured with EPL picosecond laser, and another component of long-life time was monitored with microsecond flash xenon lamp. λ_{ex} = 340 nm, c = 5.0 × 10^{-5} M in deaerated HEX, 20 °C.

7. Spectroelectrochemistry and Chemical Oxidation Study

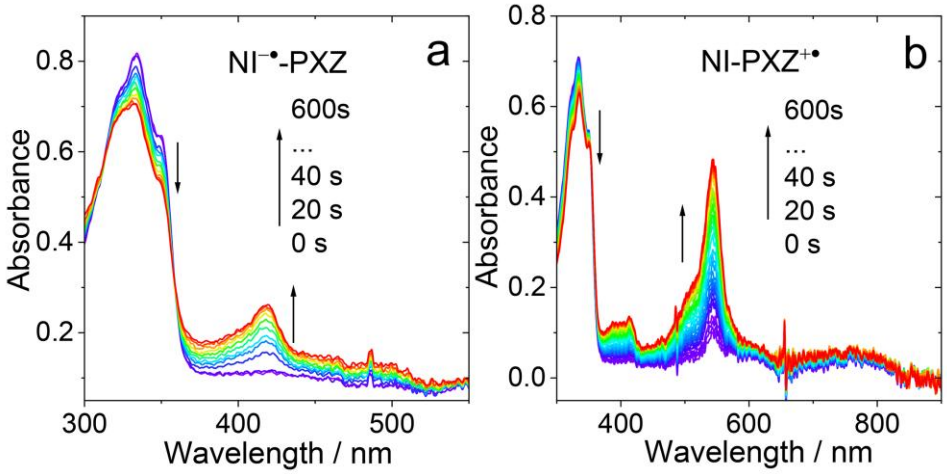

Figure S16. Spectroelectrochemical studies of **NI-PXZ**: evolution of the UV−vis absorption spectra with reduction and oxidation potentials applied, (b) upon reduction under −1.68 V, c = 5.0 × 10^{-5} M and (c) upon oxidation under +0.61 V, c = 1.0 × 10^{-4} M. The Ag/$AgNO_3$ reference electrode was used. The spectra were recorded in situ with a spectroelectrochemical cell (1 mm optical path), in deaerated DCM, 20 °C.

8. Femtosecond Time-Resolved Transient Absorption Spectra

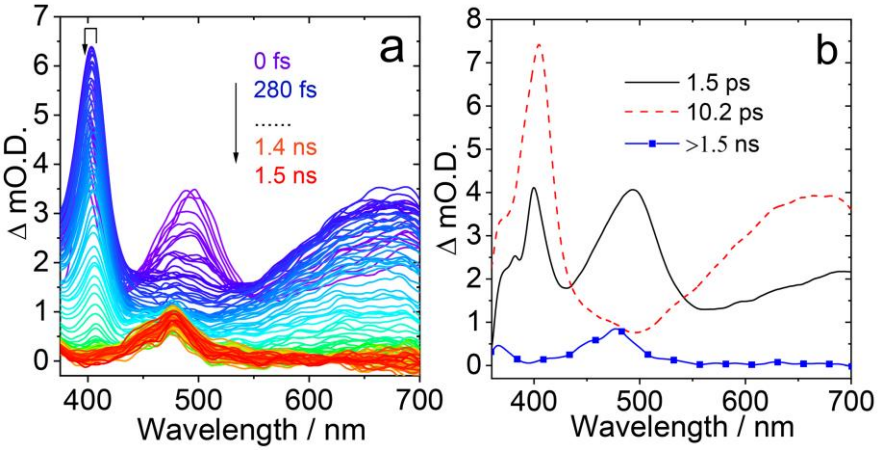

Figure S17. (a) Femtosecond transient absorption spectra of **NI-Br** in ACN, and (b) the relative EADS obtained from global analysis of the transient absorption data measured upon excitation at 350 nm.

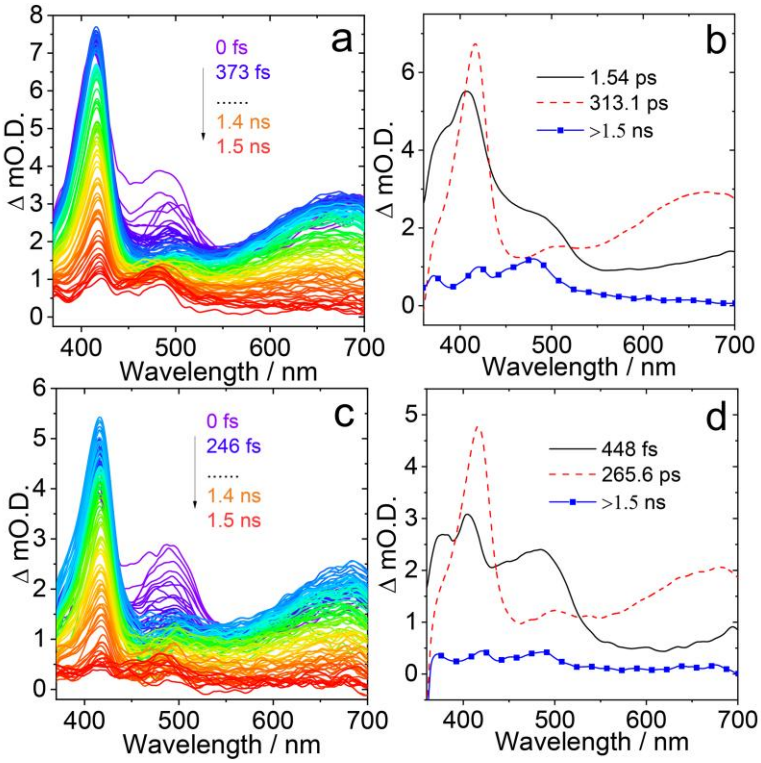

Figure S18. Femtosecond transient absorption spectra of **NI-PSeZ** in (a) TOL and (c) ACN, and the relative EADS obtained from global analysis of the transient absorption data measured in (b) TOL and (d) ACN upon excitation at 350 nm.

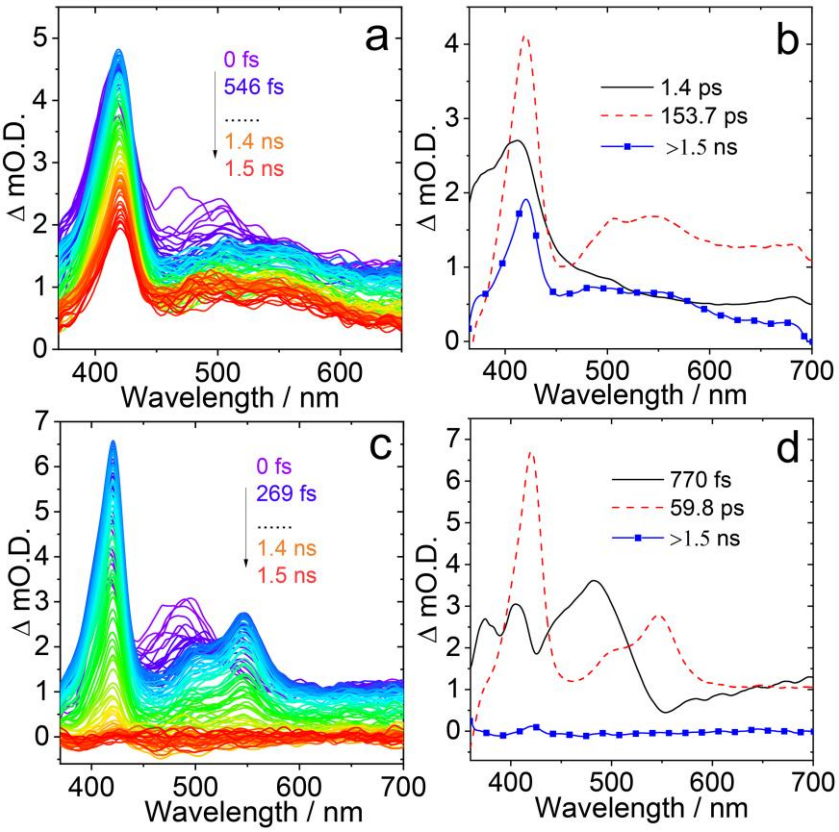

Figure S19. Femtosecond transient absorption spectra of **NI-PXZ** in (a) TOL and (c) ACN, and the relative EADS obtained from global analysis of the transient absorption data measured in (b) TOL and (d) ACN upon excitation at 350 nm.

9. Nanosecond Time-Resolved Transient Absorption Spectra

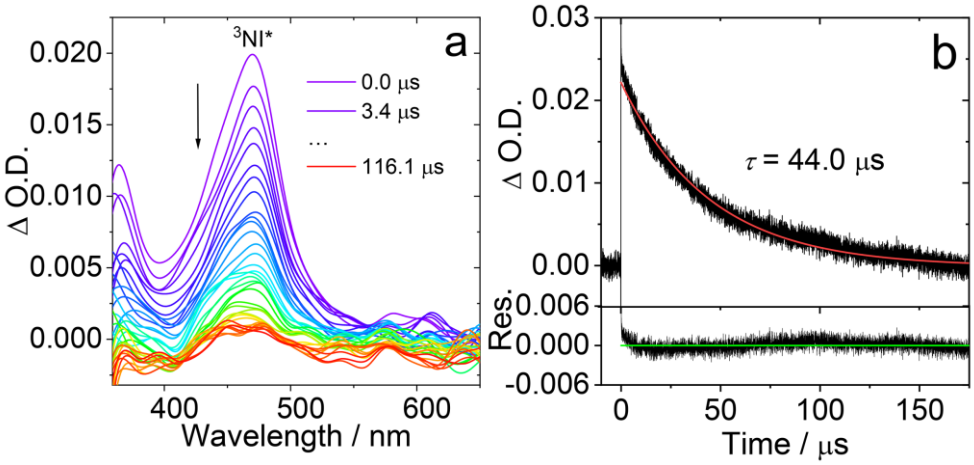

Figure S20. (a) Nanosecond transient absorption spectra of **NI-Br** in deaerated ACN (c = 2 × 10^{-5} M). (b) The corresponding decay traces are presented in 470 nm (c = 2.0 × 10^{-5} M), λ_{ex} = 355 nm, 20 °C.

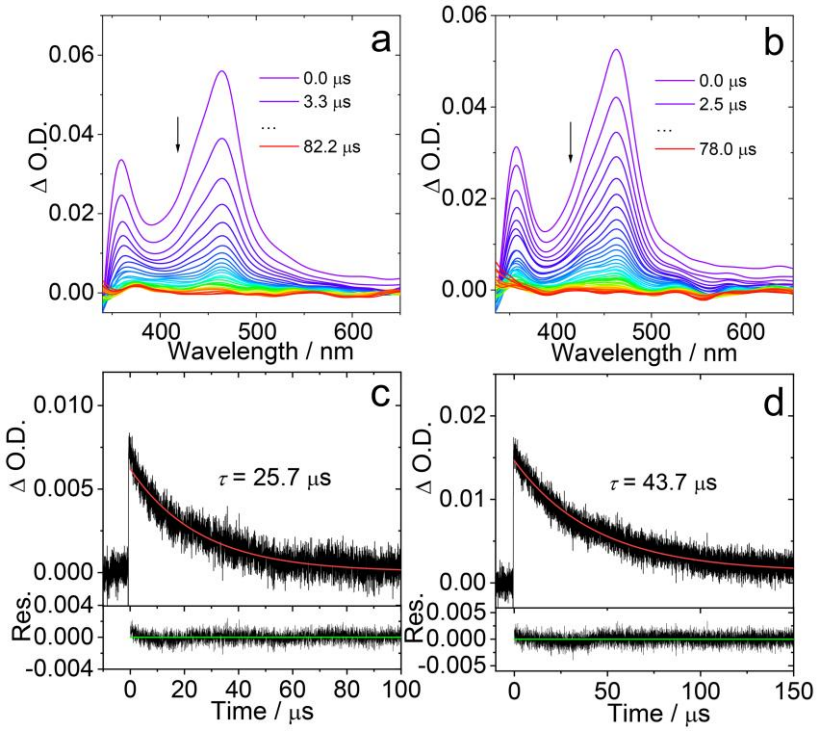

Figure S21. Nanosecond transient absorption spectra in deaerated HEX of (a) **NI-PXZ** (c = 1 × 10^{-5} M), and (b) **NI-PSeZ** (c = 1 × 10^{-5} M). The corresponding decay traces are presented in (c) 470 nm (c = 5.0 × 10^{-6} M) and (d) 470 nm (c = 5.0 × 10^{-6} M), λ_{ex} = 355 nm, 20 °C.

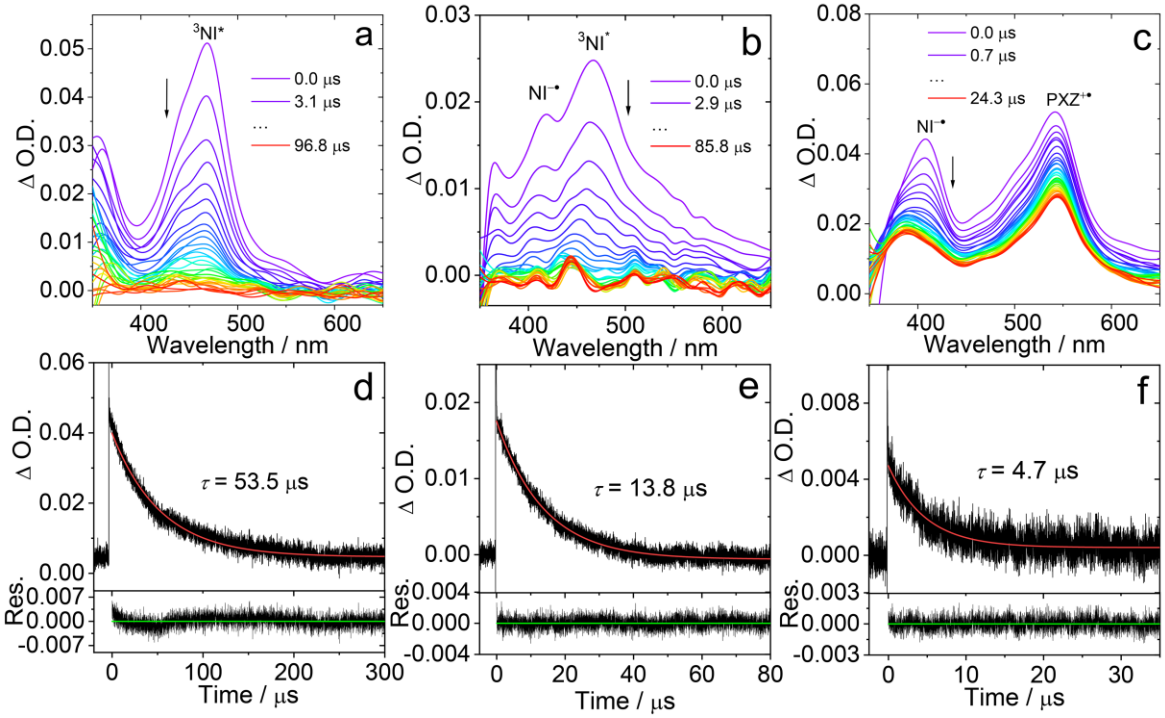

Figure S22. Nanosecond transient absorption spectra of **NI-PXZ** in different deaerated solvents of (a) CHX (c = 4.0 × 10^{-5} M), (b) TOL (c = 4.0 × 10^{-5} M), and (c) THF (c = 5 × 10^{-5} M). The corresponding decay traces are presented in (d) 470 nm (c =2.0 × 10^{-5} M), (e) 470 nm (c = 5 × 10^{-6} M), and (f) 410 nm (c = 1.0 × 10^{-5} M), λ_{ex} = 355 nm, 20 °C.

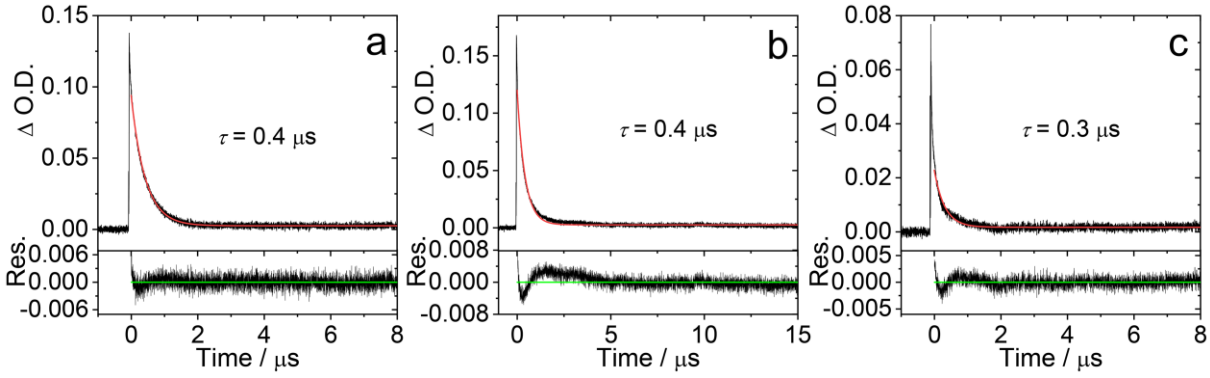

Figure S23. The corresponding decay traces of **NI-PXZ** are presented in 470 nm, (a) CHX, (b) HEX, and (c) TOL, c = 2.0 × 10^{-5} M, λ_{ex} = 355 nm, 20 °C.

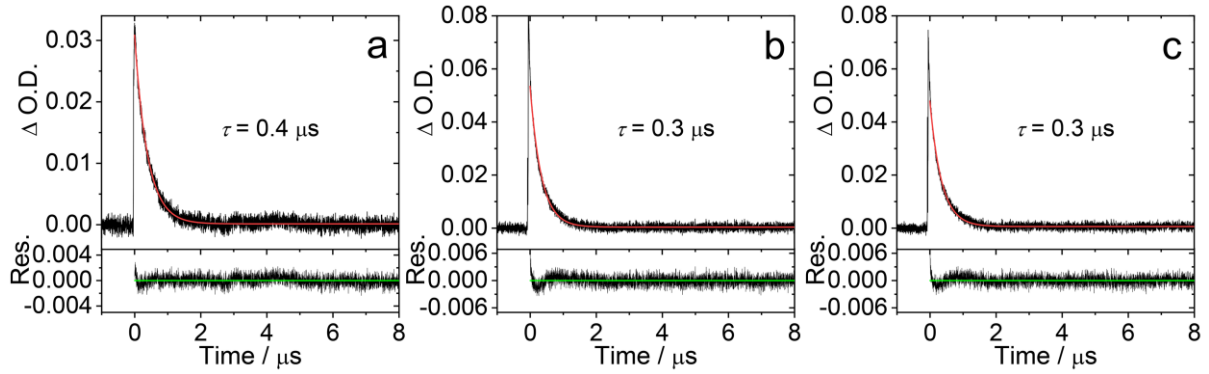

Figure S24. The corresponding decay traces of **NI-PSeZ** are presented in 470 nm, (a) CHX, (b) HEX, and (c) TOL, c = 2.0 × 10^{-5} M, λ_{ex} = 355 nm, 20 °C.

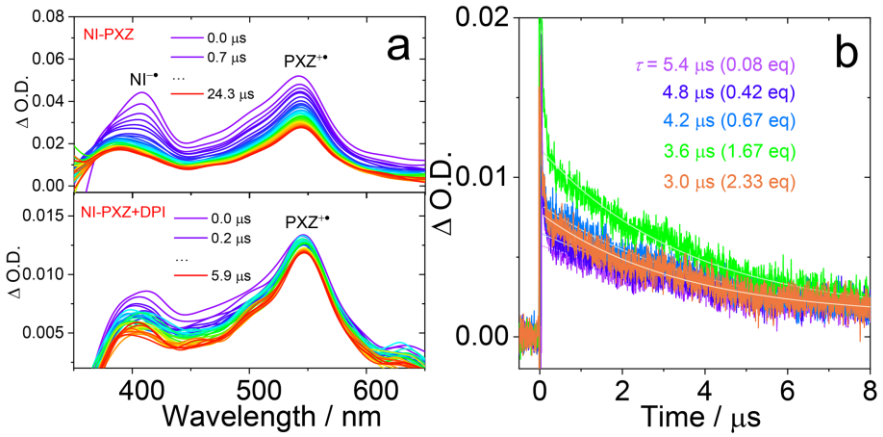

Figure S25. (a) Nanosecond transient absorption spectra of **NI-PXZ** (5.0 × 10^{-5} M) before and after addition of DPI (8.0 × 10^{-5} M) in deaerated THF. (b) The decay traces of **NI-PXZ** (1.5 × 10^{-5} M) at 410 nm upon incremental addition of DPI, λ_{ex} = 355 nm, 20 °C.

10. Theoretical Calculations

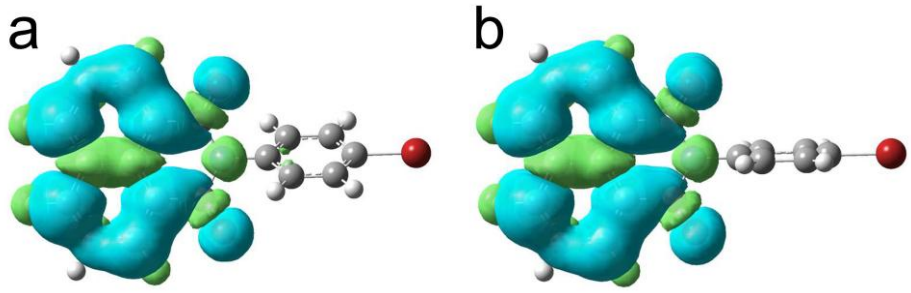

Figure S26. Calculations were performed by DFT at the CAM−B3LYP/6-31G(d) level with Gaussian 16. Triplet spin density distributions of **NI-Br** (a) in gas phase and (b) in ACN, isovalue = 0.0004.

Table S2. Electronic Excitation Energies and Corresponding Oscillator Strengths (*f*), Main Configurations, and CI Coefficients of the Low-lying Electronic Excited States of NI-PXZ and NI-PSeZ.

	Electronic transition[a]	Energy[b]	*f*[c]	CI[d]	Composition[e]
NI-PXZ	$S_0 \rightarrow S_1$	1.68 eV / 740 nm	0.0000 [f]	0.70693	H → L
	$S_0 \rightarrow S_2$	3.06 eV / 405 nm	0.0001	0.61678	H → L+1
	$S_0 \rightarrow S_3$	3.14 eV / 395 nm	0.0000 [f]	0.70689	H–1 → L
	$S_0 \rightarrow T_1$	2.33 eV / 533 nm	0.0000 [f]	0.68022	H–2 → L
	$S_0 \rightarrow T_2$	2.81 eV / 442 nm	0.0000 [f]	0.54897	H → L+5
	$S_0 \rightarrow T_3$	3.05 eV / 406 nm	0.0000 [f]	0.60938	H → L+1
NI-PSeZ	$S_0 \rightarrow S_1$	2.10 eV / 590nm	0.0000 [f]	0.70673	H → L
	$S_0 \rightarrow S_2$	3.01 eV / 412 nm	0.0000 [f]	0.70669	H–1 → L
	$S_0 \rightarrow S_3$	3.46 eV / 358 nm	0.0004	0.58306	H → L+1
	$S_0 \rightarrow T_1$	2.32 eV / 534 nm	0.0000 [f]	0.67496	H–2 → L
	$S_0 \rightarrow T_2$	3.01 eV / 412 nm	0.0000 [f]	0.70667	H–1 → L
	$S_0 \rightarrow T_3$	3.09 eV / 401 nm	0.0000 [f]	0.47264	H → L+3

[a] TDDFT//B3LYP/6-31G(d), based on the DFT//B3LYP/6-31G(d) optimized ground state geometries. [b] Only the selected low-lying excited states are presented. [c] Oscillator strengths. [d] CI coefficients are in absolute values. [e] TDDFT//B3LYP/6-31G(d) optimized excited state geometries. (D: no CT but delocalized) [f] No spin-orbital coupling effect was considered; thus, the *f* values are zero.

Table S3. SOCMEs (cm^{-1} units) in HEX and ACN for the State Pairs Evaluated at the Optimized Geometry of the Ground State.[a]

Compounds	ISC	SOCME(HEX)	ΔE^b (HEX)	SOCME(ACN)	ΔE^b (ACN)
NI-PXZ	$S_1 \rightarrow T_1$	0.00	0.00	0.00	0.00
	$S_1 \rightarrow T_2$	0.11	−0.52	0.11	−0.29
	$S_1 \rightarrow T_3$	0.06	−0.93	0.03	−0.71
	$S_1 \rightarrow T_4$	0.51	−1.25	0.52	−1.14
NI-PSeZ	$S_1 \rightarrow T_1$	0.00	0.00	0.16	0.11
	$S_1 \rightarrow T_2$	0.17	−0.12	0.00	0.00
	$S_1 \rightarrow T_3$	0.11	−0.83	0.09	−0.62
	$S_1 \rightarrow T_4$	0.51	−0.88	0.72	−0.84
NI	$S_1 \rightarrow T_1$	0.00	1.29	0.00	1.26
	$S_1 \rightarrow T_2$	0.01	0.29	0.01	0.30
	$S_1 \rightarrow T_3$	14.91	0.10	14.80	−0.09
	$S_1 \rightarrow T_4$	0.02	−0.13	0.02	−0.15
PXZ	$S_1 \rightarrow T_1$	0.00	0.77	0.01	0.77
	$S_1 \rightarrow T_2$	0.04	0.28	0.00	0.27
	$S_1 \rightarrow T_3$	0.00	0.22	0.04	0.21
	$S_1 \rightarrow T_4$	0.01	−0.15	0.00	−0.18
PSeZ	$S_1 \rightarrow T_1$	4.70	0.54	5.20	0.54
	$S_1 \rightarrow T_2$	70.69	0.17	69.40	0.15
	$S_1 \rightarrow T_3$	20.85	0.00	21.82	0.01
	$S_1 \rightarrow T_4$	7.55	−0.04	7.92	−0.04

[a] The calculation of the spin orbital coupling matrix elements (SOCMEs) were performed at B3LYP/def2-TZVP level (hexane)/(acetonitrile) using the ORCA 6.0 programs.[9] [b] $\Delta E = E(S_1) - E(T_m)$.

Table S4. Zero Field Splitting Parameters (*D* and *E*), Spin−Spin and Spin−Orbit (cm^{-1}) in HEX for the State Pairs Evaluated at the Optimized Ground State.[a]

Compounds	ZFS		SPIN−SPIN		SPIN−ORBIT	
	D / cm^{-1}	E / cm^{-1}	D / cm^{-1}	E / cm^{-1}	D / cm^{-1}	E / cm^{-1}
NI-PXZ	−0.03692	−0.00835	0.01930	−0.00075	−0.05622	−0.00760
(exp.)[b]	(0.0826)	(0.0042)				
NI-PSeZ	2.40410	0.27385	0.00620	−0.00242	2.38701	0.27230
(exp.)[b]	(0.0820)	(0.0049)				
NI	0.03627	0.00043	−0.02066	0.02496	0.05692	−0.02453
(exp.)[b]	(0.0824)	(0.0042)				
PXZ	0.03557	0.00381	0.07049	0.00015	−0.03493	0.00366
(exp.)[b]	(0.1246)	(0.0129)				
PSeZ	−9.84714	−2.13093	0.01536	−0.00859	−9.86068	−2.12174
(exp.)[b]	(0.1063/0.0820)	(0.0165/0.0049)				

[a] The calculation of the zero field splitting parameters (ZFS), spin−spin and spin−orbit were performed at B3LYP/EPR-II level (hexane) using the ORCA 6.0 programs.[9] [b] Exp. data of compounds were measured with Q−band EPR spectrometer excited with 355 nm laser and simulated by EasySpin package.

Table S5. Zero Field Splitting Parameters (*D* and *E*), Spin−Spin and Spin−Orbit (cm^{-1}) in ACN for the State Pairs Evaluated at the Optimized Ground State.[a]

Compounds	ZFS		SPIN−SPIN		SPIN−ORBIT	
	D / cm^{-1}	E / cm^{-1}	D / cm^{-1}	E / cm^{-1}	D / cm^{-1}	E / cm^{-1}
NI-PXZ	−0.06000	−0.01030	0.00184	−0.00159	−0.06184	−0.00872
(exp.)[b]	(0.0826)	(0.0042)				
NI-PSeZ	−11.19947	−0.93032	−0.00097	0.00062	−11.19171	−0.92830
(exp.)[b]	(0.0820)	(0.0049)				
NI	0.03224	0.00169	−0.01911	0.02512	0.05134	−0.02343
(exp.)[b]	(0.0824)	(0.0042)				
PXZ	0.03575	0.00224	0.07016	−0.00122	−0.03441	0.00346
(exp.)[b]	(0.1246)	(0.0129)				
PSeZ	−8.72836	−2.05922	0.01507	−0.00869	−8.74106	−2.04974
(exp.)[b]	(0.1063/0.0820)	(0.0165/0.0049)				

[a] The calculation of the zero field splitting parameters (ZFS), spin−spin and spin−orbit were performed at B3LYP/EPR-II level (acetonitrile) using the ORCA 6.0 programs.[9] [b] Exp. data of compounds were measured with Q−band EPR spectrometer excited with 355 nm laser and simulated by EasySpin package.

11. References

1. G. M. Sheldrick, Acta Crystallogr. *Sect. A: Found. Adv.*, 2008, **64**, 112–122.
2. J. J. Snellenburg, S. Laptenok, R. Seger, et al., *J. Stat. Softw.*, 2012, **49**, 1–22.
3. S. Stoll and A. Schweiger, *J. Magn. Reson.*, 2006, **178**, 42–55.
4. M. J. Frisch, G. W. Trucks, H. B. Schlegel, et al., *Wallingford, CT.*, **2016**.
5. C. Cremer, M. Goswami, C. K. Rank, et al., *Angew. Chem., Int. Ed.* 2021, **60**, 6451–6456.
6. C. Cremer, M. A. Eltester, H. Bourakhouadar, et al., *Org. Lett.* 2021, **23**, 3243–3247.
7. Y. Wu, X. Chen, Y. Mu, et al., *Dyes Pigm.* 2019, **169**, 81–88.
8. X. Xiao, Y. Yan, A. A. Sukhanov, et al., *J. Phys. Chem. B*, 2023, **127**, 6982–6998.
9. F. Neese, *WIREs Comput. Mol. Sci.* 2025, **15**, e70019.